Energy Dissipation versus Delay Tradeoffs in a Buffer-aided Two-hop Link

Chen Dong, Li Li, Bo Zhang, Lie-Liang Yang and Lajos Hanzo

School of ECS, University of Southampton, SO17 1BJ, United Kingdom

Tel: 0044-(0)23-8059 3364, Email:

{cd2g09,ll5e08,bz2g10,lly,lh}@ecs.soton.ac.uk, http://www-mobile.ecs.soton.ac.uk

Abstract

In this contribution, we study the trade-off between energy dissipation and delay in a buffer-aided two-hop link. First, the optimality of a two-dimensional Transmission Activation Probability Space (TAPS) partitioning is shown formally boh in the presence and absence of an outage region. Then, the relationship between the packet energy dissipation and the block delay is found, which is established with the aid of a buffer state transition matrix. Moreover, the concept of 'artificial outage' is introduced and applied for striking a trade-off between the energy dissipation and block delay. Then an algorithm is provided for finding the matching block delay and energy dissipation pairs. Our analysis and performance results showed that the proposed methods outperform all other methods, resulting in a reduced average packet delay and reduced energy dissipation.

Index Terms

Cooperative communication, opportunistic routing, buffer, energy consumption, dissipation, channel space, delay.

The financial support of the European Research Council under the auspices of its Advanced Fellow Grant is gratefully acknowledged.

I. INTRODUCTION

Mitigating the energy dissipation is one of the key goals in contemporary wireless communications research. It may benefit both the telecommunications operators in terms of a cost reduction and the mobile users in terms of an extended battery recharge period. Naturally, the classic relaying technique, which reduces the single-hop transmission span should be considered [1, 2]. However, it may impose an increased delay. The trade-offs between the throughput and delay were discussed in [3, 4]. As a further advance, in this paper, we discuss the trade-off between the energy dissipation and delay in a buffer-aided system conceived for near-capacity transmission.

The buffer-aided multihop transmission regime relying on activating the most appropriate link from the set of all links was proposed in [5–7]. In [5, 6], a multi-hop link (MHL) is assumed to have buffers for temporarily storing the received packets. Hence, the RNs are operated under the so-called Store-and-Forward (SF) relaying scheme. As a benefit of storing packets at the RNs, during each time-slot (TS) the best hop having the highest signal-to-noise ratio (SNR) can be activated from the set of those hops that have packets awaiting transmission in the buffer. A packet is then transmitted over the best hop. Later, this buffer-aided transmission regime was combined with adaptive modulation in [8]. The authors of [9, 10] also discussed buffer-aided systems, which were characterized with the aid of queuing theory. The buffer-aided systems are also capable of enhancing the security of communications [11].

However, the cost of achieving the above-mentioned buffer-aided benefits is an increased delay. As mentioned in [12, 13], there are two basic types of delay: *block delay* and *packet delay*. The block delay is defined as the time required for a block of packets generated by the source node (SN) to reach the destination node (DN), which is inversely proportional to the throughput. By contrast, the packet delay is the time required for delivering a specific packet from the SN to the DN, when assuming that there is an infinite number of packets ready for transmission in the buffers. Buffer-aided multi-hop transmission has the same block delay as the conventional multi-hop transmission scheme of [14]. This is because both schemes transmit a single packet over a single hop per TS. By contrast, the packet delay is a random variable, which is distributed across a dynamic range bounded by the minimum and maximum

packet delays. We assume that the minimum delay is two TSs in the two-hop link, while the maximum delay is infinite. In this paper, we concentrate our attention on the trade-off between the block delay (throughput) and the average end-to-end normalized packet energy dissipation (PED). The authors of both [9] and [15] observed the trade-off between the packet delay and the capacity. Therefore, we will consider these methods as our reference.

Achieving low-complexity, yet accurate channel estimation [16], for near-capacity communication is becoming realistic. Explicitly, based on turbo or LDPC codes as well as EXIT-chart aided designs [17], it is possible to have a vanishingly low BER when the received SNR is higher than a near-capacity threshold. The state-of-the-art was summarized in [18]. Near-capacity communications allows us to jointly design the upper layers and the physical-layer forward error correction (FEC), therefore it makes our discussions practical at the packet level.

The remainder of this paper is organized as follows. Section II presents our system model followed by the concept of TAPS. The optimality of the TAPS concept is shown in Section III. The optimization of the channel activation scheme under a delay-constraint is proposed in Section IV, while in Section V we provide our numerical and simulation results. Finally, our conclusions are offered in Section VI.

II. System Model

The system model under consideration is a typical two-hop wireless link [12–14], which is shown in Fig. 1. This model is portrayed in the next three sections in terms of its buffering scheme, the physical layer and the transmission scheme.

A. Buffering at the RN

The two-hop link consists of three nodes, a SN, a buffer-aided Relay Node (RN) and a DN. The distance from the SN to the RN is d_1, while the distance from the RN to the DN is d_2. We assume that the RN is capable of storing a maximum of B packets and that the classic Decode-and-Forward (DF) protocol [19] is employed for relaying the signals. Note that if no packets are stored in the RN, the RN-DN channel must not be activated. By contrast, if the buffer at the RN is full, the SN-RN channel must not be activated. Finally, each node

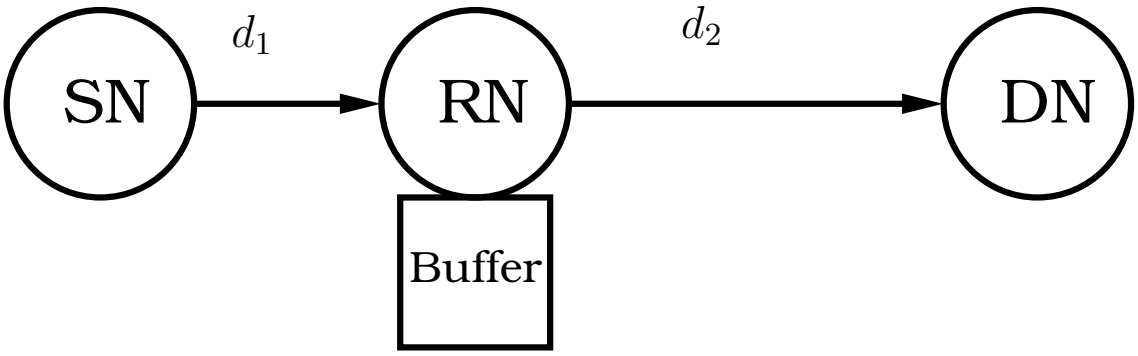

Fig. 1. System model for a two-hop wireless link, where source node SN sends messages to destination node DN via RN node.

is capable of adjusting its transmit power between zero and the maximum transmit power P_{max}.

B. Physical Layer

In this paper, a near-capacity [20] FEC scheme is assumed, so that the BER becomes vanishingly low when the received SNR exceeds a near-capacity threshold. Therefore, we assume that the receiver is capable of perfectly decoding the transmitted packet, when the receiver's SNR is higher than a specific SNR threshold γ_{T_h}. Based on this assumption and on the knowledge of the instantaneous CQ, the transmitter adjusts its transmit power for ensuring that the required SNR of γ_{T_h} is indeed achieved at the receiver. Hence, the transmit power required is inversely proportional to the instantaneous CQ.

In our system, only a single packet is transmitted in a time slot. [1] The channels are assumed to experience independent block-based flat Rayleigh fading, where the complex-valued fading envelope of a hop remains constant within a TS, but it is independently faded for different TSs, which is ensured for example by using frequency hopping. In addition to the fading model, the pathloss is assumed to obey the negative exponential law of $d^{-\alpha}$, where α is the pathloss exponent having a value between 2 to 6. It is also assumed that the instantaneous

[1]Practical measurements showed that the average of the 90% of the coherence time is typically around 30ms for fixed wireless communication and 3ms for a vehicular velocity of 70km/h [21]. Based on these measurements, it is reasonable to partition the time into Time Slots (TS) and to assume that the channel is quasi-static within a TS.

channel fading values are denoted by γ_{SR} and γ_{RD}. The instantaneous transmit power $\mathcal{E}_{SD}$, $\mathcal{E}_{RD}$ or $\mathcal{E}_{RD}$ of each node can then be calculated with the aid of $\kappa = 9.895 \times 10^{-05}$ and the noise power of $N = 10^{-14}W$ which corresponds to a receiver sensitivity of $-110dBm$. An example of calculating $\mathcal{E}_i, i = SR, RD$ is given by

$$\mathcal{E}_i = \frac{\gamma_{T_h}}{\gamma_i}\frac{d_i^{\alpha}N}{\kappa} = \frac{\bar{\gamma}_i^{rec}}{\gamma_i},\ \mathcal{E}_i \leq P_{max}, \tag{1}$$

where $\bar{\gamma}_i^{rec} = \frac{\gamma_{T_h} d_i^{\alpha} N}{\kappa}$. An outage event will occur, when the receiver's SNR becomes lower than γ_{T_h}, despite using the maximum transmission power of P_{max}, therefore we have

$$P_{max} = \frac{\gamma_{T_h}}{\gamma_{SR}^{out1}}\frac{d_{SR}^{\alpha}N}{\kappa} = \frac{\gamma_{T_h}}{\gamma_{RD}^{out1}}\frac{d_{RD}^{\alpha}N}{\kappa}, \tag{2}$$

where γ_{SR}^{out1} and γ_{RD}^{out1} are defined as the Type 1 outage thresholds[2] of the corresponding channel. Assuming that each packet contains $\mathcal{I}$ information per bit, the Type 1 outage thresholds γ_{SR}^{out1} and γ_{RD}^{out1} may be calculated based on Shannon's capacity formula of $\mathcal{I} = \log 2(1+\gamma_{T_h})$ and (2).

C. Transmission Scheme

The proposed transmission scheme has two stages. The first stage is constituted by the system analysis, which is carried out before any real data transmission. Based on all our assumptions and on the independent parameters, all dependent parameters, including the key parameters of γ_{SR}^{out2}, γ_{RD}^{out2} and E_{ffe} may be calculated, leading to our theoretical performance results. In the second stage, simulations are carried out with the aid of all the parameters used in the first stage. Our studies are based on the following assumptions:

- The SN always has information to send, hence the system operates in its steady state.
- Both the SN S and DN D can store an infinite number of packets. By contrast, each of the limited-complexity RN can only store at most B packets.
- The MAC layer protocol conceived [8] for our multihop diversity scheme can be applied here for supporting the link-activation process. In the following, let us assume that the RN knows the channel qualities of both the SN-RN and the RN-DN channels. Based on the specific channel activation method to be considered in the next two sections, the RN will inform all other nodes to activate the corresponding link.

[2]The type of outage will be detailed later.

III. Review of TAPS and Proof its Optimality

The concept of TAPS was firstly introduced in our previous papers [22–24]. Although we proposed and applied the TAPS concept in several scenarios, the optimality of TAPS has not been formally shown. Here, we systematically revisit the TAPS concept and prove its optimality. TAPS is an analysis tool, which relies on a specific metric. In this paper, the Packet Energy Dissipation (PED) is adopted as our optimization cost-function or metric. For other metrics, such as the capacity, please see Appendix-A for a reference. In order to augment the relevant concept as explicitly as possible, three examples of a two-hop link are shown below. We commence from a two-hop link having a RN exactly in the middle and conclude by outlining the rationale of our non-linear channel space partitioning.

The first example is a simple one relying on the conventional buffer-aided selection combining (SC) philosophy, where the link having the highest SNR is activated. Again, we consider a two-hop link with $d_1 = d_2$, as shown in Fig. 1. In the two hops, the receive SNRs γ_{SR}^{rec} and γ_{RD}^{rec} are given by the product of the corresponding instantaneous channel fading values (γ_{SR}, γ_{RD}) and the related average receive SNRs ($\bar{\gamma}_{SR}$, $\bar{\gamma}_{RD}$), respectively. The pair of instantaneous channel fading values (γ_{SR} and γ_{RD}) form a so-called channel space, as shown in Fig. 3(a). The X-axis represents the fading value γ_{SR} of the SN-RN channel, while the Y-axis represents the fading value γ_{RD} of the RN-DN channel. In each time slot, the instantaneous fading values of both the SN-RN (γ_{SR}) and of the RN-DN (γ_{RD}) channels map to a specific point $(\gamma_{SR}, \gamma_{RD})$ in the 2D channel space. Obviously, if the mapped point is in the region below the OE line, because we have $\gamma_{RD} < \gamma_{SR}$, then the SN-RN link should be activated. By contrast, if the mapped point is in the region above the OE line, because $\gamma_{RD} > \gamma_{SR}$, then the RN-DN link should be activated. The boundary is the OE line and the slope of it is one. The activation probabilities of the two hops are identical, because both channels obey the same distribution. Therefore, the system can be operated in its **steady** state.

The second example discusses a buffer-aided two-hop link associated with non-identical average receive SNRs, because the RN is not half-way between the SN and DN. Let us assume that the average receive SNR $\bar{\gamma}_{SR}$ of the SN-RN channel is higher than the average receive SNR $\bar{\gamma}_{RD}$ of the RN-DN channel. If the channel having the higher received channel

SNR ($\bar{\gamma}_{SR}\gamma_{SR}$ or $\bar{\gamma}_{RD}\gamma_{RD}$) is activated, the boundary of the two activation regions should be the OE_0 line seen in Fig. 3(b). However, the area of the region encompassed by the points $\gamma_{SR}OE_0$ is higher than that of the other region determined by $EP\gamma_{RD}$. Therefore, the activation probability of the two hops is different and the system operates in an unstable mode, potentially leading to a buffer overflow.

In order to allow the system to operate in its steady state rather than in the unstable mode of E_0 seen in Fig. 3(b), there are two plausible methods of adjusting the boundary OE_0:

a) If we force the boundary OE_0 to be linear, OE_0 should be moved back to OE. However, this method is not optimum;

b) If the OE_0 boundary is non-linear.

Let us discuss the second method directly, which is more beneficial than the first method, because we may arrive at an optimum boundary, as detailed below.

In order to elaborate on the process of transmission-probability adjustment, let us partition the TAPS into perfectly tiling squares, as shown in Fig. 2. The light-grey region represents the activation-region of the SN-RN channel, while the dark-grey region represents that of the RN-DN channel. Now, the activation probability of the SN-RN channel is higher. Let us now move some of the dark-grey tiles to the light-grey region, albeit we realize that this is achieved at a performance penalty, as detailed below.

When considering a tile ΔS, the question arises: what is the energy dissipation ($\mathcal{E}_{\Delta S \in SR}$) caused by ΔS, when ΔS belongs to the activation region of the SN-RN hop? This is quantified as

$$\mathcal{E}_{\Delta S \in SR} = p_{\Delta S} \left(\frac{C_{SR}}{\gamma_{SR}} \right), \tag{3}$$

where, $p_{\Delta S}$ is the probability of the point $(\gamma_{SR}, \gamma_{RD})$ falling into the ΔS region of Fig. 2, C_{SR} is a constant value and $\frac{C_{SR}}{\gamma_{SR}}$ indicates that the energy dissipation imposed is inversely proportional to the channel quality experienced. By contrast, what is the energy dissipation ($\mathcal{E}_{\Delta S \in RD}$) caused by ΔS, when ΔS belongs to the activation region of the RN-DN hop? This is given by

$$\mathcal{E}_{\Delta S \in RD} = p_{\Delta S} \left(\frac{C_{RD}}{\gamma_{RD}} \right), \tag{4}$$

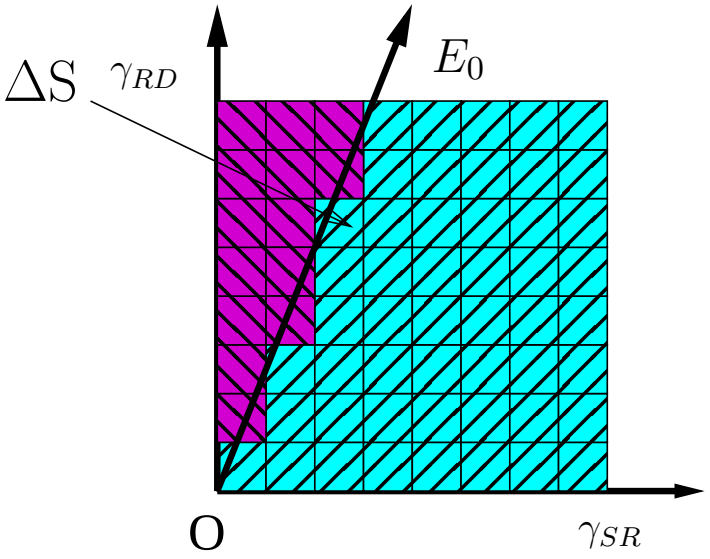

Fig. 2. The transmission activation probability space (TAPS) of a two-hop link, where the average receive SNR of the SN-RN hop and of the RN-DN hop are non-identical. The transmission activation probability space is partitioned into tiles.

where, C_{RD} is a constant value and again, $\frac{C_{RD}}{\gamma_{RD}}$ indicates that the energy dissipation is inversely proportional to the RN-DN SNR encountered. If the region ΔS is reassigned from the SN-RN channel to the RN-DN channel, how much extra energy in dissipated? This is quantified by $\mathcal{E}_{\Delta S \in RD} - \mathcal{E}_{\Delta S \in SR}$, which should be as low as possible. Then the transmission probability is modified by $p_{\Delta S}$. Therefore, the power-dissipation cost of this probability adjustment is

$$E_{ffe} = \frac{\mathcal{E}_{\Delta S \in RD} - \mathcal{E}_{\Delta S \in SR}}{p_{\Delta S}} \tag{5}$$

$$= \frac{C_{RD}}{\gamma_{RD}} - \frac{C_{SR}}{\gamma_{SR}}. \tag{6}$$

By contrast, if we are willing to tolerate a higher energy-dissipation penalty for the sake of having the same transmit probability for the unequal-SNR links, the OE_0 boundary may be reshaped, as seen in Fig. 3(b).

In order to allow the two-hop link to operate in its steady state, we may continue increasing E_{ffe}, until the probability represented by the region $\gamma_{SR}OE_2$ becomes the same as that represented by $E_2O\gamma_{RD}$. In this reassignment process, the tiles imposing a lower E_{ffe} are adjusted firstly, followed by those imposing a higher power-dissipation penalty E_{ffe}, until the above-mentioned condition is satisfied. Let us now show formally that this boundary is

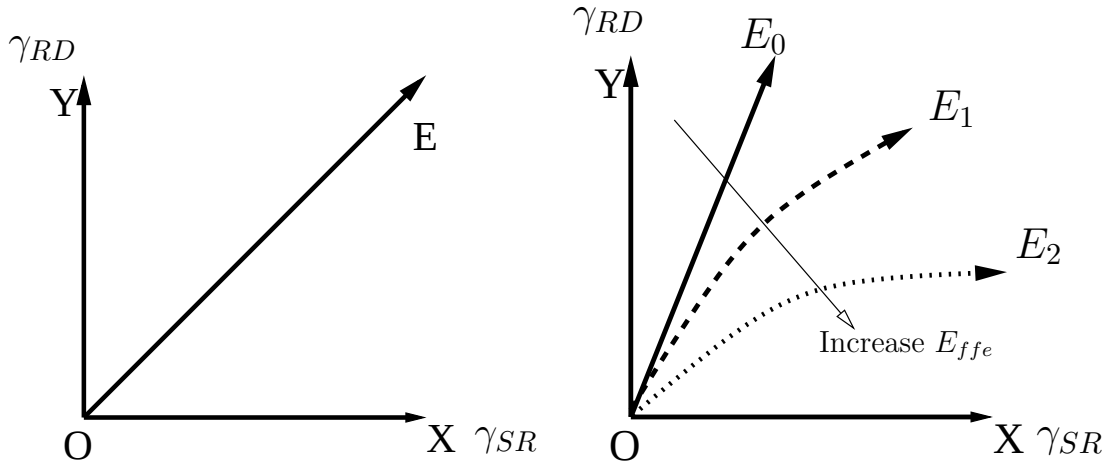

(a) (b)

Fig. 3. (a), the TAPS of a two-hop link, where the average SN-RN channel SNR $\bar{\gamma}_{SR}$ and the average RN-DN channel SNR $\bar{\gamma}_{RD}$ are identical. (b), the TAPS (plane) of a two-hop link, where the SN-RN channel and the RN-DN channel are non-identical. The transmission-probability boundary is reshaped for various values of E_{ffe}.

optimal.

In Fig. 4(a), the TAPS is now partitioned into unequal tiles by assuming that each tile represents the same probability. The fading envelope of the channel usually does not obey a uniform distribution. In order to allow each tile to represent the same probability, the area of each tile may be different. **Below we will show that the boundary OE_2 is optimum by invoking the method of contradiction.**

Contradiction statement: Let us assume that there is an optimal TAPS partitioning, which is different from the partitioning OE_2 seen in Fig. 3(b) and 4(a). Due to this assumption, the energy dissipation of this partitioning is lower than that of the partitioning OE_2 seen in Fig. 3(b).

Due to having the same probability of encountering the regions of $\gamma_{SD}OE_2$ and $E_2O\gamma_{RD}$, there are $N(N > 0)$ tiles in the region $E_2O\gamma_{RD}$ representing the activation of the SN-RN hop, while there are also N tiles in the region $\gamma_{SD}OE_2$ corresponding to the activation of the RN-DN hop. Let us now consider a specific pair of them (say ΔS_{1A} and ΔS_{2A}), as shown in Fig. 4(a). Correspondingly, there is a tile ΔS_{1B} on the boundary OE_2, which has the same X coordinate value as ΔS_{1A}. Similarly, there is also a tile ΔS_{2B} on the boundary OE_2, which has the same Y coordinate value, as ΔS_{2A}. Let us now consider three different actions:

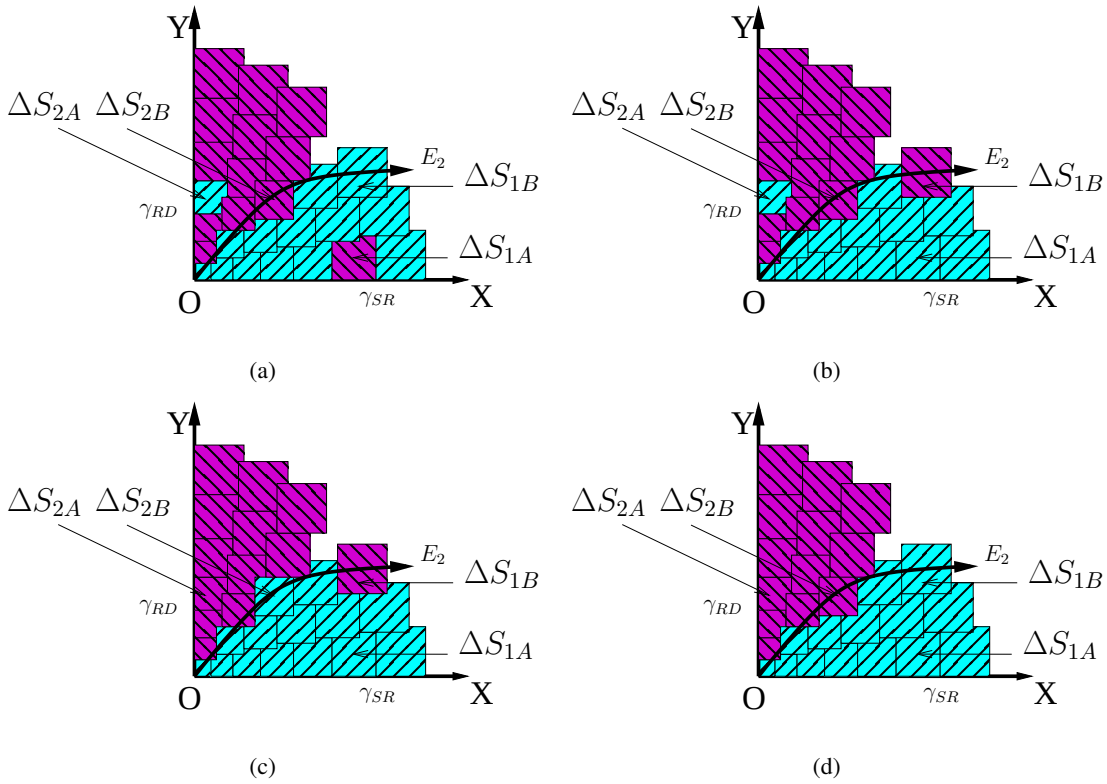

Fig. 4. The TAPS (plane) of a two-hop link, where the SN-RN channel and the RN-DN channel are non-identical. The TAPS is partitioned into many small tiles, each of which has the same probability. Compared to (a), the TAPS affiliation of ΔS_{1A} and ΔS_{1B} has been exchanged in (b). Then, the TAPS affiliation of ΔS_{2A} and ΔS_{2B} has been exchanged in (c). In (d), both the tiles ΔS_{1B} and ΔS_{2B} are on the boundary OE_2. Hence exchanging the TAPS affiliation of ΔS_{2A} and ΔS_{2B} does not affect the energy dissipation.

1) exchange the affiliation of ΔS_{1A} and ΔS_{1B} by remapping them between the two parts of the TAPS;

2) exchange the affiliation of ΔS_{2A} and ΔS_{2B};

3) exchange the affiliation of ΔS_{1B} and ΔS_{2B}.

This has the same transmit probability effect, as exchanging the affiliation of ΔS_{1A} and ΔS_{2A}, but their energy-dissipation effects are rather different, when compared to 'no action'. To elaborate a little further, if we exchange the TAPS affiliation of ΔS_{1A} and ΔS_{1B}, as shown in Fig. 4(b), the activation probability of each hop remains the same. However, the energy dissipation is reduced due to the fact that the energy dissipated within the tile ΔS_{1B} of Fig. 4(b) is lower than that within ΔS_{1A} of Fig. 4(a), because γ_{RD} is higher for ΔS_{1B} than for ΔS_{1A}, while the energy dissipated by the SN-RN hop remained the same due to having the same γ_{SD} ordinate values both for ΔS_{1A} and for ΔS_{1B}.

Similarly, if we exchange the TAPS affiliation of ΔS_{2A} and ΔS_{2B} as shown in Fig. 4(c), the activation probability of each hop remains the same. However, the energy dissipation is reduced due to the fact that the energy dissipated within the tile ΔS_{2B} of Fig. 4(c) is lower than that of ΔS_{2A} in Fig. 4(b), while the energy dissipated by the RN-DN hop remained the same during the above process, since both ΔS_{2A} and ΔS_{2B} have the same γ_{RD} ordinate values.

Lastly, both the tiles ΔS_{1B} and ΔS_{2B} are on the boundary OE_2, as shown in Fig. 4(d). Hence, exchanging the TAPS affiliation of ΔS_{2A} and ΔS_{2B} does not affect the energy dissipation. Following the above three actions, the TAPS affiliation of the tiles ΔS_{1A} and ΔS_{2A} was exchanged and the energy dissipation imposed was decreased. The energy dissipation of the partitioning seen in Fig. 4(d) is lower than that observed in Fig. 4(a) and the probabilities represented by the light-grey and dark-grey tiles are the same in both figures. This however contradicts to the statement that there is a better boundary than OE_2, which demonstrates that the tile-based partitioning seen in Fig. 4(a) is not optimal. Therefore, no better tile-based TAPS partitioning can be found than OE_2.

IV. Optimization of the link Activation under a Delay-Constraint

In the previous section, the TAPS concept was revisited and its optimality was proven. However, this reliability improvement is achieved at the cost of an increased delay. Our basic idea is to adjust the values of the elements in the Markov State Transition Matrix (MSTM) $\boldsymbol{T}$. The original concept of 'State' and MSTM were proposed in the context of buffer-aided systems in [5, 13, 23–25]. Upon assuming that the buffer size of the RN is B packets, its state is defined as $S_b = b$, when b packets are stored in the RN. Therefore, the total number of states is $(B+1)$. Given $(B+1)$ states, a state transition matrix denoted by $\boldsymbol{T}$ can be populated by the state transition probabilities $\{\boldsymbol{T}_{i,j} = P(s(t+1) = S_j | s(t) = S_i),\ i, j = 0, 1, \ldots, B\}$. This adjustment will affect two specific relationships, as shown in Fig. 5. In the following, firstly the relationship between the MSTM $\boldsymbol{T}$ and the average packet delay is derived. Then the minimum PED may be designed based on the MSTM $\boldsymbol{T}$. Lastly, an algorithm will be conceived for finding the input values of the MSTM $\boldsymbol{T}$.

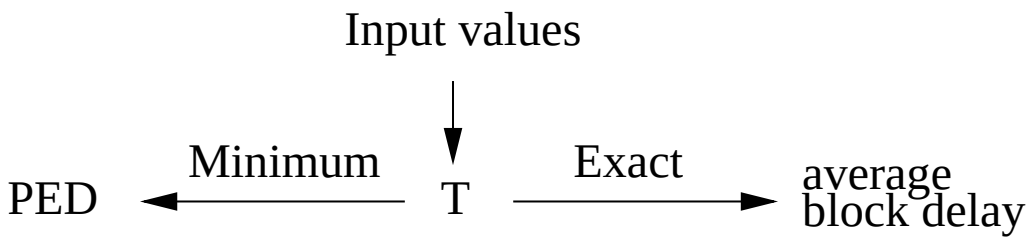

Fig. 5. Based on the existing values input into $\boldsymbol{T}$, both the PED and the block delay may be obtained.

A. *Relationship Between the MSTM $\boldsymbol{T}$ and Block Delay*

Having obtained the MSTM $\boldsymbol{T}$, the steady-state transmission probabilities can be computed according to [15, 26] as

$$\boldsymbol{\pi} = \boldsymbol{T}^T \boldsymbol{\pi}, \tag{7}$$

where we have $\boldsymbol{\pi} = [\pi_0, \pi_1, \ldots, \pi_B]^T$ and π_i is the steady-state probability that the 2-hop link is in state S_i [2]. The steady-state probability of a state is applied as the expected value of the probability of this specific state in the system. The knowledge of the steady-state probability of every state allows us to determine the Probability Mass Function (PMF) of the buffer occupancy.

Based on our assumptions, in each row of the MSTM $\boldsymbol{T}$, there are up to three non-zero values, representing the probability of activating the first/second hop or the probability of the outage event. Let us define the outage probability as $\boldsymbol{T}_{i,i}, i = 0, \cdots, B$ when there are i packets in the buffer and the probability of activating the first hop is $\boldsymbol{T}_{i,i+1}, i = 1, \cdots, (B-1)$, when there are i packets in the buffer. Naturally, the probability of activating the second hop is the remaining complementary probability in each row of the MSTM $\boldsymbol{T}$. Therefore, the MSTM $\boldsymbol{T}$ may be expressed as

$$\boldsymbol{T} = \begin{bmatrix} T_{0,0} & 1-T_{0,0} & & & & & \\ T_{1,0} & T_{1,1} & T_{1,2} & & & & \\ & T_{2,1} & T_{2,2} & T_{2,3} & & & \\ & & \ddots & \ddots & \ddots & & \\ & & & \ddots & \ddots & \ddots & \\ & & & & 1-T_{B,B} & T_{B,B} \end{bmatrix}, \tag{8}$$

where we have $T_{i,i-1} = 1 - T_{i,i} - T_{i,i+1}, i = 1, \cdots, (B-1)$. Upon substituting (8) into (7), the $\pi_i, i = 0, \cdots, B$ values may be obtained as follows:

$$\begin{cases} \tilde{\pi}_B = \Pi_{i=0}^{B-1} T_{i,i+1} \\ \tilde{\pi}_j = \Pi_{i=0}^{j-1} T_{i,i+1} \Pi_{i=j}^{B-1} T_{i+1,i}, \quad j = 1, \cdots, (B-1) \\ \tilde{\pi}_0 = \Pi_{i=0}^{B-1} T_{i+1,i} \qquad\qquad\qquad , \end{cases} \tag{9}$$

where we have

$$\pi_j = \frac{\tilde{\pi}_j}{\sum_{i=0}^{B} \tilde{\pi}_i}. \tag{10}$$

Proof: See Appendix-B

Finally, the block delay D_{blc} and the end-to-end throughput Φ may be expressed as

$$\Phi(\boldsymbol{T}) = \frac{1}{D_{blc}}(\boldsymbol{T}) = \sum_{i=1}^{B} \pi_i T_{i,i-1}. \tag{11}$$

B. Relationship Between the MSTM $\boldsymbol{T}$ and the PED

Having determined the relationship between the MSTM $\boldsymbol{T}$ and the block delay, let us now discuss the relationship between $\boldsymbol{T}$ and PED. In each time slot, only a single row in $\boldsymbol{T}$ is in use. In each row of $\boldsymbol{T}$, there are upto three non-zero values representing the activation probability of the SN-RN hop, of the RN-DN hop and the outage probability. Therefore the key problem is how to partition the TAPS with the aid of these probabilities.

In Section III, we proved that the activation boundary is optimal, when there is no outage region. When we do have an outage region, it may be classified into two types. Type 1: the outage occurs due to having low channel qualities. The corresponding probability is formulated as $T_{i,i}^{out1} = (1 - e^{-\gamma_{SR}^{out1}})(1 - e^{-\gamma_{RD}^{out1}})$; Type 2: the channel qualities are adequate, but an 'artificial outage' is declared in order to reduce the energy dissipation. The total outage probability $T_{i,i}, i = 0, \cdots, B$ is the sum of the Type 1 and Type 2 outage probabilities. Now we claim that the outage region in the TAPS is a rectangle.

Proof: See Appendix-C.

Theoretically, the final optimal TAPS partitioning is shown in Fig. 6. The coordinates of the upper-left corner are defined as $(\gamma_{SR}^{out2}, \gamma_{RD}^{out2})$. The region 'Odeg' represents the Type 1 outage region for the SN-RN hop, while the upper-left corner of the total outage region is moving along with 'elck' upon increasing the Type 2 outage region. The region 'Oach'

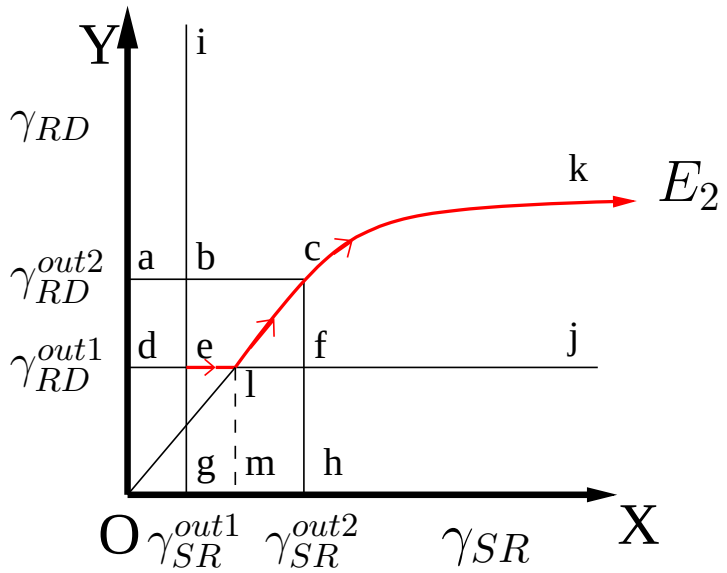

Fig. 6. The TAPS of a two-hop link with Type 1 outage region 'Odeg'. Then with the increasing of the Type 2 outage region, the total outage region enlarges from 'Odeg' to 'Odlm', then 'Oach', and so on. As shown in Appendix-C that the outage region is always a rectangular with the upper-left corner along the 'elck' line. The region 'Oach' is the outage region, the activation region of the SN-RN hop is 'Xhck', while the activation region of the RN-DN hop is 'Ykca'.

exemplifies the outage region, while the activation region of the SN-RN hop is 'Xhck' and that of the RN-DN hop is 'Ykca'.

In the following, let us firstly consider when the upper-left corner of the total outage region is on the line 'lck'. In this TAPS partitioning, we have three parameters: γ_{SR}^{out2}, γ_{RD}^{out2} and E_{ffe}. The following equations give the unique solutions for these three parameters. The probability represented by the region 'Oach' is

$$(1-e^{-\gamma_{SR}^{out2}})(1-e^{-\gamma_{RD}^{out2}})=T_{i,i}. \tag{12}$$

The point 'c' is on the boundary E_2, yielding

$$\frac{\bar{\gamma}_{RD}^{rec}}{\gamma_{RD}^{out2}}-\frac{\bar{\gamma}_{SR}^{rec}}{\gamma_{SR}^{out2}}=E_{ffe}. \tag{13}$$

When we have $E_{ffe}\geq 0$, the probability represented by 'Xhck' is

$$\int_{\gamma_{SR}^{out2}}^{\infty} e^{-\gamma}(1-e^{-\frac{\bar{\gamma}_{RD}^{rec}}{\frac{\bar{\gamma}_{SR}^{rec}}{\gamma}+E_{ffe}}})d\gamma=T_{i,i+1}. \tag{14}$$

By contrast, if we have $E_{ffe}<0$, the curve Ock bends towards the Y-axis. Therefore the

probability representing the activation of the SN-RN hop is given by:

$$T_{i,i+1} = \int_{\gamma_{SR}^{out2}}^{\frac{-\bar{\gamma}_{SR}^{rec}}{E_{ffe}}} e^{-\gamma}(1 - e^{-\frac{\bar{\gamma}_{SR}^{rec}}{\frac{\bar{\gamma}_{SR}^{rec}}{\gamma}+E_{ffe}}})d\gamma + e^{-\frac{\bar{\gamma}_{SR}^{rec}}{E_{ffe}}}. \tag{15}$$

Theoretically, the three unknowns may be found based on (12) to (14) or (12), (13) and (15). From a practical perspective, a computationally efficient method is required, which may be found in Appendix-D.

If the upper-left corner of the total outage region is on the line 'el', we have $\gamma_{RD}^{out2} = \gamma_{RD}^{out1}$ and

$$\gamma_{SR}^{out2} = -\ln\left(1 - \frac{T_{i,i}}{1 - e^{-\frac{\gamma_{RD}^{out1}}{\bar{\gamma}_{RD}^{rec}}}}\right). \tag{16}$$

Having γ_{SR}^{out2} and γ_{RD}^{out2}, the last unknown E_{ffe} may be found based on the activation probabilities of the two hops, which relies on the same principle, as mentioned in the context of Fig. 3(b).

Given the knowledge of the ith row of $\boldsymbol{T}$ ($\boldsymbol{T}_i$) and the key parameters, the energy dissipation of the SN-RN and the RN-DN hops may be readily obtained. If the upper-left corner of the total outage region is on the line 'lck' and we have $E_{ffe} \geq 0$, then the corresponding energy dissipations are

$$\mathcal{E}_{SR,i}(\boldsymbol{T}_i) = \int_{\gamma_{SR}^{out2}}^{\infty} \frac{\bar{\gamma}_{SR}^{rec}}{\gamma} e^{-\gamma}(1 - e^{-\frac{\bar{\gamma}_{RD}^{rec}}{\frac{\bar{\gamma}_{SR}^{rec}}{\gamma}+E_{ffe}}})d\gamma \tag{17}$$

$$\begin{aligned}\mathcal{E}_{RD,i}(\boldsymbol{T}_i) = &\int_{\gamma_{RD}^{out2}}^{\frac{\bar{\gamma}_{RD}^{rec}}{E_{ffe}}} \frac{\bar{\gamma}_{RD}^{rec}}{\gamma} e^{-\gamma}(1 - e^{-\frac{\bar{\gamma}_{SR}^{rec}}{\frac{\bar{\gamma}_{RD}^{rec}}{\gamma}+E_{ffe}}})d\gamma \\ &+ \int_{\frac{\bar{\gamma}_{RD}^{rec}}{E_{ffe}}}^{\infty} \frac{\bar{\gamma}_{RD}^{rec}}{\gamma} e^{-\gamma}d\gamma.\end{aligned} \tag{18}$$

Similar procedures can also be used for other scenarios. The total energy dissipation of both hops associated with $\boldsymbol{T}_i$ is given by the sum of each hops' consumption, yielding

$$\mathcal{E}_i(\boldsymbol{T}_i) = \mathcal{E}_{SR,i}(\boldsymbol{T}_i) + \mathcal{E}_{RD,i}(\boldsymbol{T}_i). \tag{19}$$

Finally, the total energy dissipation of the system is given by:

$$\mathcal{E}(\boldsymbol{T}) = \sum_{i=0}^{B} \pi_i \mathcal{E}_i(\boldsymbol{T}_i). \tag{20}$$

C. Finding the Input Values of the MSTM $\boldsymbol{T}$

Having determined the relationship between $\boldsymbol{T}$-PED and $\boldsymbol{T}$-D_{blc}, our next ambition is to find an optimal MSTM $\boldsymbol{T}$, which should provide the minimum PED for a given D_{blc}. However, there are $(3B+1)$ non-zero values in $\boldsymbol{T}$, hence it is quite a challenge to find the optimal solution. To make progress, Algorithm 1 based on the classic greedy algorithm was conceived for finding suboptimal, but beneficial solutions. The output of this algorithm is a series of $\boldsymbol{T}^{(k)}, k=1,\cdots$, corresponding to a number of PED-D_{blc} pairs.

Algorithm 1: The algorithm of finding the MSTM $\boldsymbol{T}$.

1 Initiation: Set $T_{0,0}^{(1)}=1-e^{-\gamma_{SR}^{out1}}$, $T_{0,1}^{(1)}=1-T_{0,0}^{(1)}$; $T_{i,i-1}^{(1)}=1-e^{-\gamma_{RD}^{out1}}$, $T_{i,i}^{(1)}=T_{i,i}^{out1}$, $T_{i,i+1}^{(1)}=1-T_{i,i}^{(1)}-T_{i,i-1}^{(1)}$, $i=1,\cdots,(B-1)$; $T_{B,B}^{(1)}=1-e^{-\gamma_{RD}^{out1}}$, $T_{B,B-1}^{(1)}=1-T_{B,B}^{(1)}$. Set Δ to a small number. $k=1$;

2 Calculate $\mathcal{E}(\boldsymbol{T}^{(1)})$ and $D_{blc}(\boldsymbol{T}^{(1)})$ based on (11) and (20);

3 **while** $D_{blc}(\boldsymbol{T}^{(k)})$>$10\min(D_{blc})$ **do**

4 **for** *i=all non-zero values in* $\boldsymbol{T}^{(k)}$ **do**

5 $\boldsymbol{Ttemp}^{(k,i)}=\boldsymbol{T}^{(k)}$;

6 Increase Δ for the ith non-zero value in $\boldsymbol{Ttemp}^{(k,i)}$;

7 Decrease Δ for other values in the same row in $\boldsymbol{Ttemp}^{(k,i)}$;

8 Calculate $\mathcal{E}(\boldsymbol{T}^{(k,i)})$ and $D_{blc}(\boldsymbol{T}^{(k,i)})$;

9 **end**

10 Find the index i' of $\min\left(\frac{D_{blc}^{(k,i)}-D_{blc}^{(k)}}{\mathcal{E}(\boldsymbol{T}^{(k)})-\mathcal{E}(\boldsymbol{T}^{(k,i)})}|\mathcal{E}(\boldsymbol{T}^{(k)})>\mathcal{E}(\boldsymbol{T}^{(k,i)})\right)$;

11 $\boldsymbol{T}^{(k+1)}=\boldsymbol{T}^{(k,i')}$, $\mathcal{E}(\boldsymbol{T}^{(k+1)})=\mathcal{E}(\boldsymbol{T}^{(k,i')})$ and $D_{blc}(\boldsymbol{T}^{(k+1)})=D_{blc}(\boldsymbol{T}^{(k+1,i')})$;

12 k=k+1;

13 **end**

In Algorithm 1, the initiation of the MSTM $\boldsymbol{T}$ is set in line 1. In order to find a lower block delay, all the outage probabilities $T_{i,i}$ are set as small as possible, while all activation probabilities $T_{i,i-1}$ of the RD hop are set as high as possible. Naturally, the activation probabilities of the SR hop are the complementary probabilities. In line 3, the algorithm will be terminated, when the current block delay is 10 times higher than its minimum value,

which may be considered as the upper bound of the practical region. From line 4 to 9, one of the non-zero elements of the MSTM $\boldsymbol{T}$ is increased by a unit step Δ, while the other probabilities in the same row should be decreased. The corresponding PED and block delay are also calculated. In line 10, the index of the minimum ratio of the block delay increment and of the PED increment is found. Lastly, Algorithm 1 updates the MSTM $\boldsymbol{T}$, $\mathcal{E}(\boldsymbol{T})$ and $D_{blc}(\boldsymbol{T})$.

V. Performance Results

In this section, we provide a range of numerical and/or simulation results for characterizing both the energy dissipation and the MSTM $\boldsymbol{T}$ of the buffer-aided two-hop link considered in order to illustrate the effects of the probability adjustments in the MSTM $\boldsymbol{T}$. In all experiments, the SN is at the position $[100m, 100m]$, while DN is at the position $[1100m, 100m]$. The parameters of N, κ, P_{max} and pathloss alpha are $N = 10^{-14}$, $\kappa = 9.895 \times 10^{-05}$, $P_{max} = 0.0003Watt$ and $\alpha = 3$. We set $\mathcal{I} = 1$, which implies that the threshold is 0dB. In Fig. 7 to 10, the legend 'Sim' indicates that the results are from simulations, while the legend 'The' means that the results are from our theoretical analysis.

Given a row of the MSTM $\boldsymbol{T}$, the TAPS partitioning may be calculated based on Section IV-B, before the simulations commence. Once the simulations have been started, the instantaneous fading values $(\gamma_{SR}, \gamma_{RD})$ may be directly mapped to a specific point in a region of the TAPS. The corresponding link will then be activated. The first set of results seen in Fig. 7 characterizes the impact of the RN's buffer size both on the PED and on the block delay. The X-coordinate represents the block delay, while the Y-coordinate represents the PED. The curves marked by the cross, star and plus markers represent the PED-D_{blc} relationship evaluated from Algorithm 1 as well as from (11) and (20). Observe in Fig. 7 that as expected, the PED performance improved upon increasing the buffer size. These results are also compared to four existing transmission protocols. Specifically, the *Starving the Buffer* (SB) and the *Limiting the Queue Size* (LQS) regimes constitute a pair of protocols proposed in [9] for striking a delay-performance trade-off. In the SB protocol, the channel activation criterion remains the same, regardless of the buffer occupancy in the RN while in the LQS protocol, a trade-off is struck based on the adjustment of the buffer size. Both

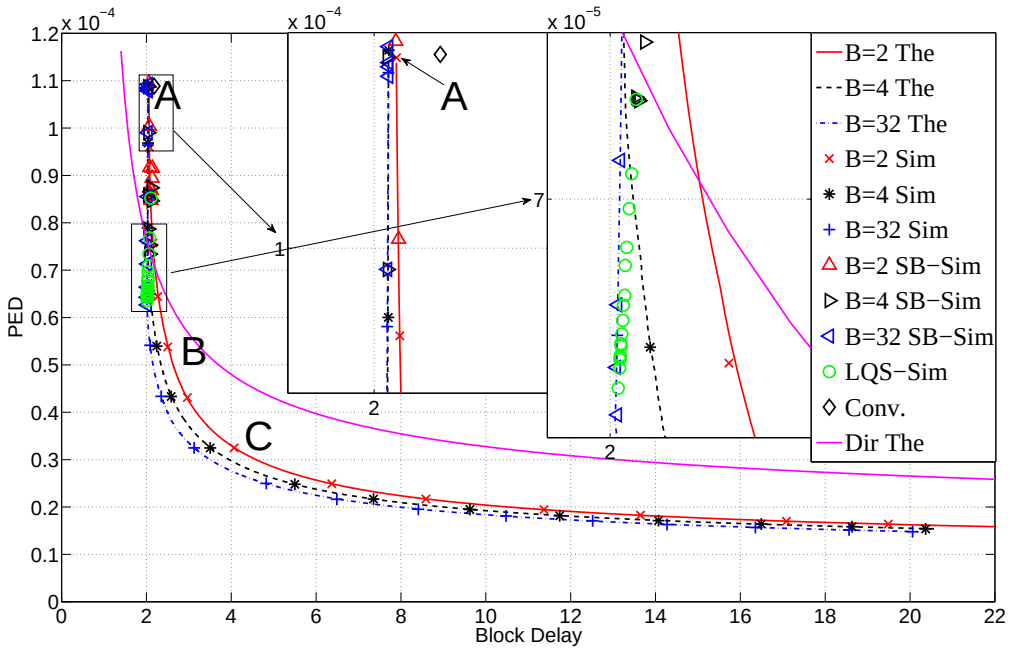

Fig. 7. The PED and the block delay relationship evaluated from (11), (20) and Algorithm 1. The results are compared to four other protocols.

the SB and LQS protocols disregard the Type 2 outages, therefore the corresponding trade-off region is limited. Additionally, a conventional buffer-aided transmission protocol (Conv.) was proposed in [14]. The data of the SN was firstly transmitted to the RN and then it was relayed to the DN. This protocol has a fixed PED-D_{blc} relationship and it is distinguished by the diamonds in Fig. 7. For all two-hop relaying protocols, the block delay was found to be higher than 2, while it may be lower than two for the classic direct transmission (Dir) associated with a higher PED. The Dir curve is associated with a Type 2 outage and it exhibits a worse performance than our proposed method for $D_{blc} > 2.01$.

Fig. 8 characterizes the updating of the elements in the MSTM $\boldsymbol{T}$, when the buffer size is B=2. The X-coordinate represents the adjustment index when we have $\Delta = 0.01$ in Algorithm 1, while the Y-coordinate represents the element values in the MSTM $\boldsymbol{T}$. Observe in Fig. 8 that all outage probabilities ($\boldsymbol{T}_{i,i}, i = 0, 1, 2$) were increased, while the transmission probabilities of both hop1 and hop2 were reduced.

Fig. 9 shows the distribution of the packet delay, when stipulating the same MSTM $\boldsymbol{T}$ at the point A, B and C seen in Fig. 7. The theoretical results obtained from the algorithm in

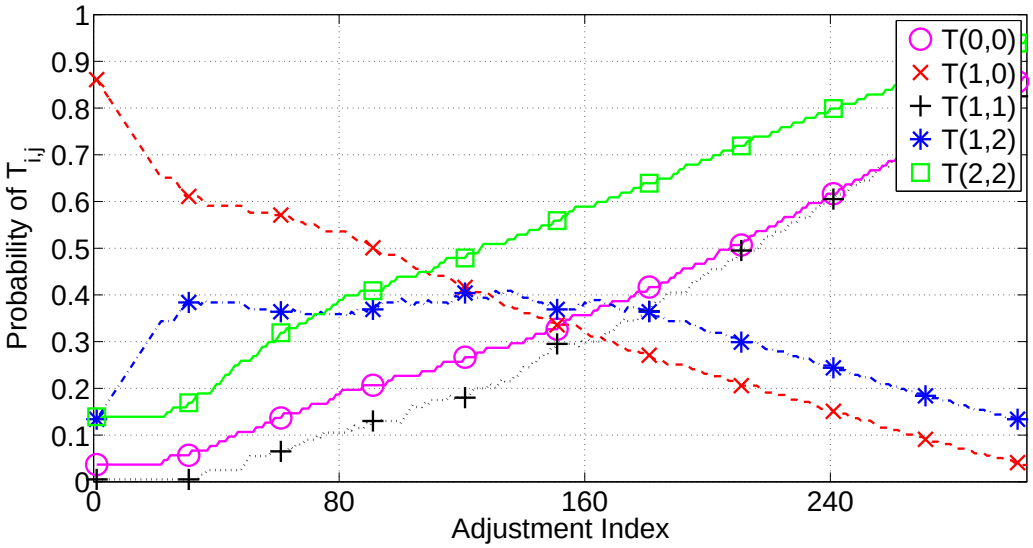

Fig. 8. Updating the element values in the MSTM $\boldsymbol{T}$ during the running of Algorithm 1.

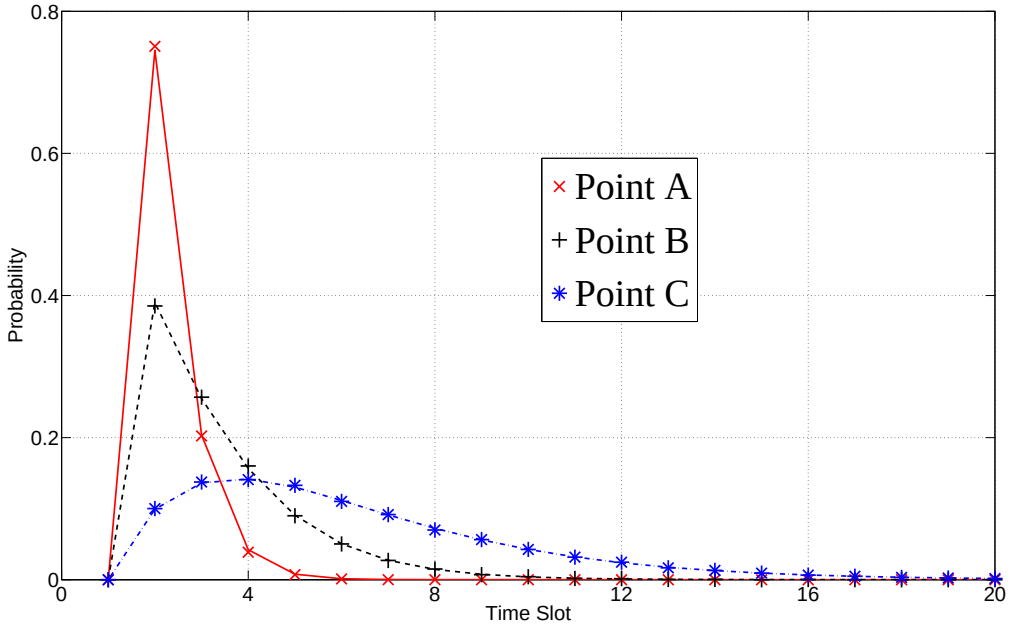

Fig. 9. The distribution of the packet delay theoretically evaluated from the algorithm in [8] and confirmed by simulations.

[8] are represented by the lines, while the simulation results are represented by the markers. It is clear from Fig. 9 that the probability of long packet delays was increased, when the PED reduced.

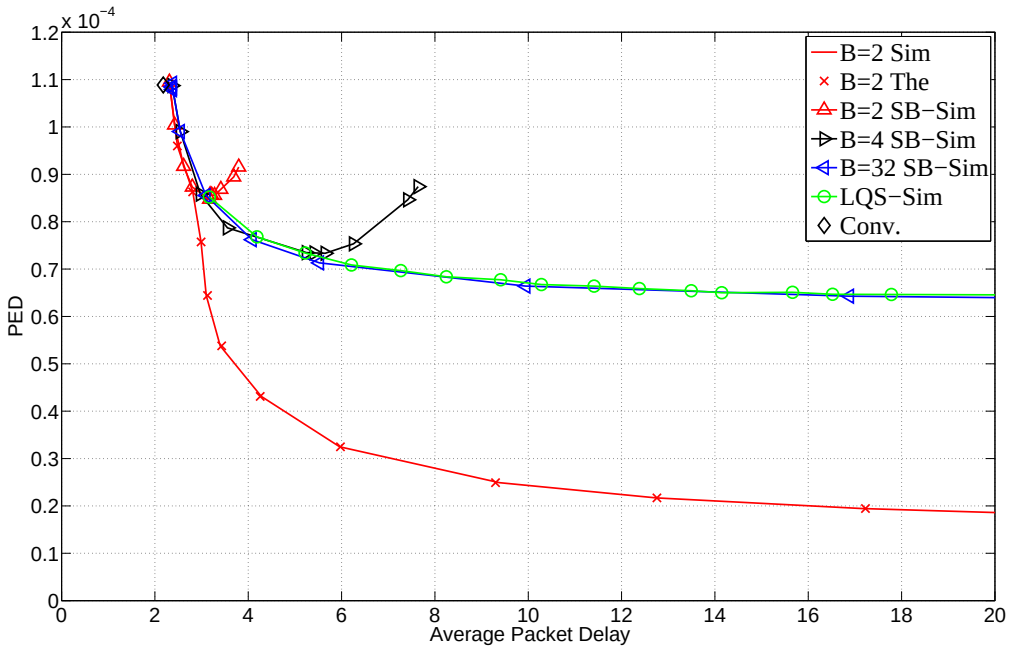

Fig. 10. The relationship between the PED and the average packet delay, which was evaluated from the algorithm in [8] and confirmed by simulations. The Results are compared to the simulation results evaluated by three other protocols.

Fig. 10 characterizes the relationship between the PED and the average packet delay. There are two methods of evaluating the average packet delay. Firstly, it can be evaluated from the PMF of the packet delay, which may be obtained from the algorithm advocated in [8]. The other method is based on Little's Law and on the distribution of the buffer fullness, as mentioned in (36) of [9]. In order to arrive at a precise expression, the first method is preferred. Observe in Fig. 10 that our proposed method outperforms both the SB, LQS and the Conv. protocol for $D_{blc} > 3$.

VI. Conclusions

In this contribution, the optimality of TAPS partitioning associated with two activation regions and an outage region has been proven. Based on this proof, the relationship between the MSTM and the minimum PED as well as the block delay may be evaluated. Moreover,

the concept of 'artificial outage' was applied in order to strike a trade-off between the energy dissipation and block delay. Then an algorithm was conceived for finding the sub-optimal, but beneficial block delay and PED pairs. Our analysis and performance results showed that the proposed methods significantly reduced the energy dissipation, even for a small buffer. Our future research will concentrate on finding the minimum block delay both with and without an energy dissipation constraint in a more complex network.

APPENDIX

A. Appendix-A

In Section III, we proved the optimality of TAPS using an energy dissipation metric. By contrast, let us now consider the capacity as our metric. We will show that the TAPS provides optimal results, as in [9].

Let us consider the same scenario as in Fig. 1. Given the initial boundary E_0 in Fig. 4(a), the capacity C_{SR} of the SN-RN hop is higher then the capacity C_{RD} of the RN-DN hop. The end-to-end capacity C_{SD} is given by the smaller value of C_{SR} or C_{RD}. The difference between C_{SR} and C_{RD} is $(C_{SR}-C_{RD})$. Similar to (3) and (4), if the region ΔS is assigned to the SN-RN or the RN-DN hop, the corresponding capacity difference caused by reassigning ΔS is given by $\Delta C_{SR} = p_{\Delta S}\log_2(1+\bar{\gamma}_{SR}^{rec}\gamma_{SR})$ and $\Delta C_{RD} = p_{\Delta S}\log_2(1+\bar{\gamma}_{RD}^{rec}\gamma_{RD})$, respectively. If ΔS is reassigned from the SN-RN hop to the RN-DN hop, how much is the capacity difference reduced between the two hops? This is given by

$$\begin{aligned}&\Delta(C_{SR}-C_{RD})\\ =&p_{\Delta S}\left[\log_2(1+\bar{\gamma}_{SR}^{rec}\gamma_{SR})+\log_2(1+\bar{\gamma}_{RD}^{rec}\gamma_{RD})\right].\end{aligned} \tag{21}$$

Since the end-to-end capacity is defined as the smaller of the values of C_{SR} or C_{RD}, the increment value of the end-to-end capacity is given by $p_{\Delta S}[\log 2(1+\bar{\gamma}_{RD}^{rec}\gamma_{RD})]$. Therefore the ratio of the capacity increment to the capacity difference reduction is

$$E_{ffe} = \frac{p_{\Delta S}[\log 2(1+\bar{\gamma}_{RD}^{rec}\gamma_{RD})]}{\Delta(C_{SR}-C_{RD})}. \tag{22}$$

Note that during the reassignment process, we wish to increase the capacity as much as possible, which should be considered as the denominator, while ensuring that the capacity

difference between the links becomes as slow as possible, which should be considered as the numerator.

Based on the same procedure and the same algorithm as mentioned in Section III, the optimal TAPS boundary may be found. Zlatanov *et. al* [9] solved this problem with the aid of queuing theory and as expected, we arrive at the same boundary. More explicitly, if we set

$$\frac{-\log_2(1+\bar{\gamma}_{RD}^{rec}\gamma_{RD})}{\log_2(1+\bar{\gamma}_{SR}^{rec}\gamma_{SR})}=\mu, \tag{23}$$

and

$$E_{ffe}=\frac{-1}{\rho}, \tag{24}$$

then we arrive at (18) of [9]. However, the TAPS relies on a different method, which is easier to interpret physically and may be more readily applied to diverse metrics, such as the energy dissipation metric.

B. Find π_j

[3]Following from (7), the jth $j=2,\cdots,(B-2)$ equation can be expressed as

$$\pi_j=\pi_{j-1}T_{j-1,j}+\pi_jT_{j,j}+\pi_{j+1}T_{j+1,j}. \tag{25}$$

Upon substituting (9) and (10) into the right hand side of (25), we have

$$\begin{aligned}
&\pi_{j-1}T_{j-1,j}+\pi_jT_{j,j}+\pi_{j+1}T_{j+1,j} && (26)\\
=&\frac{1}{\sum_{i=0}^{B}\tilde{\pi}_i}\left(\Pi_{i=0}^{j-2}T_{i,i+1}\Pi_{i=j-1}^{B-1}T_{i+1,i}T_{j-1,j}\right.\\
&+\Pi_{i=0}^{j-1}T_{i,i+1}\Pi_{i=j}^{B-1}T_{i+1,i}T_{j,j}\\
&\left.+\Pi_{i=0}^{j}T_{i,i+1}\Pi_{i=j+1}^{B-1}T_{i+1,i}T_{j+1,j}\right) && (27)\\
=&\frac{\Pi_{i=0}^{j-1}T_{i,i+1}\Pi_{i=j}^{B-1}T_{i+1,i}}{\sum_{i=0}^{B}\tilde{\pi}_i}\underbrace{\left(T_{j,j-1}+T_{j,j}+T_{j,j+1}\right)}_{=1} && (28)\\
=&\pi_j. && (29)
\end{aligned}$$

[3]In Appendix-B of [27], the authors suggested the reversibility of the related Markov Chain. Although a Markov Chain having symmetric state transition matrix is indeed reversible, the general Markov Chain dose not obey reversibility. Moreover in [27], $\boldsymbol{A}$ is a symmetric matrix based on Eq. (8-9). Therefore, the chain is reversible and Appendix-B of [27] may be further simplified from $\pi_i\boldsymbol{A}_{i,j}=\pi_j\boldsymbol{A}_{j,i}$ to $\pi_i=\pi_j$ and finally we have $\pi_i=\frac{1}{(L+1)^K}, i=1,\cdots,(L+1)^K$.

Based on a similar procedure, the solution may also be readily found for $j = 0, 1, (B-1), B$. The solution is unique due to the fact that we have the same number of unknowns as well as equations and $\det |\boldsymbol{T}| \neq 0$.

C. Optimal Partitioning for a Pair of Known Activation Probabilities and an Outage Probability

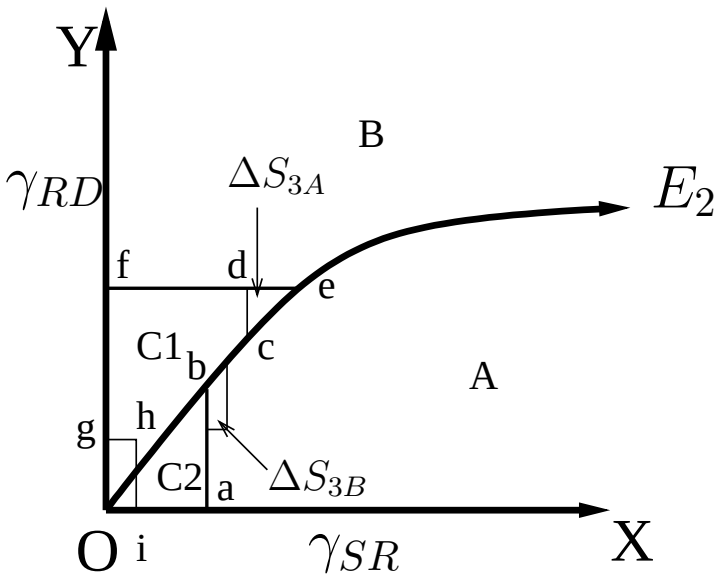

Fig. 11. The TAPS of a two-hop link with Type 2 outage region. The outage region is C1 and C2. The regions A and B represent the SN-RN or the RN-DN hops are activated.

In TAPS, the boundary between a single outage region and a single transmission region should be a straight line, otherwise the convex and the concave curves may be exchanged. More explicitly, both the 'fd' and 'ba' in Fig. 11 are straight lines. Then, the Type 1 outage region is a rectangle shown as 'Oghi'. There should be two boundaries between the activation regions and the outage region. The outage region covers the Type 1 outage region based on its definition. The boundaries here are 'ba' and 'fe', while the outage region boundary is 'OfebaO'. The outage region is a rectangle, which implies that the boundaries between the outage region and the pair of activation regions share a common point. In other words 'b' and 'e' are coincident points. **Below we will show that this statement is true by invoking the method of contradiction.**

Contradiction statement: Let us assume that the two optimal boundaries do not share a common point. This situation is depicted in Fig. 11. In this figure, the outage regions are C1 and C2, while the regions A and B represent that either the SN-RN or the RN-DN hop is activated, respectively. The boundary between the activation regions and outage region are 'fe' and 'ba'. Let us consider a pair of small regions, namely ΔS_{3A} of region C1 and ΔS_{3B} of region A, which represent the same probability. Exchanging the TAPS affiliation of ΔS_{3A} and ΔS_{3B} does not affect the outage probability. On the other hand, the energy dissipation of the SN-RN hop is reduced after exchanging them. This however contradicts to the statement that 'fe' and 'ba' are two optimal boundaries, which demonstrates that the partitioning seen in Fig. 11 is not optimal. Therefore, point 'b' and 'e' should be a pair of coincident points.

An alternative interpretation of this principle is that the region having a better channel quality cannot be an outage region. Let us denote the coordinates of e by (e_x, e_y) and those of b by (b_x, b_y). The lower bound of the RD transmission region should be higher than the upper bound of the SR outage regions, which is formulated as $e_y \geqslant b_x$, while the lower bound of the SR transmission region should be higher than the upper bound of the RD outage region represented by $b_x \geqslant e_y$. Therefore, we have $e_y = b_x$.

Note that the boundary E_2 of Fig. 11, which is associated with the outage probability region may be different from the boundary without an outage probability region. However, all the procedures and the proof of optimality provided in Section III are still valid for the TAPS having an outage probability.

D. Solving Eq. (12) *to* (14)

Let us now consider an efficient method of solving equations (12) to (14). A similar procedure is also available for (12), (13) and (15).

Upon substituting (12) and (13) into (14), we arrive at (35). In the following, the closed-form expression of $\mathcal{F}$ in (35) is obtained and then we prove that $\mathcal{F}$ is a monotonically decreasing function of γ_{SR}^{out2}.

1) The closed-form expression of $\mathcal{F}$: Let us consider a more general integral of the form seen in (35), yielding

$$\mathcal{G} = \int_A^\infty e^{-B\gamma} \frac{-1}{e^{\frac{D}{\gamma}+C}} d\gamma. \tag{30}$$

Upon substituting $t = B\gamma + \frac{\gamma}{D+C\gamma}$ into (30), we have

$$\begin{aligned}\mathcal{G} =& \frac{1}{2B} e^{-(BA+\frac{A}{D+CA})} \\ &+ \frac{1}{2B} \int_{BA+\frac{A}{D+CA}}^{\infty} e^{-t} \frac{Ct+BD-1}{\sqrt{(Ct+BD-1)^2+4BD}} dt. \end{aligned} \tag{31}$$

Then, upon substituting $s = Ct + BD - 1$ and $E = CBA + \frac{CA}{D+CA} + BD - 1$ into (31), we arrive at

$$\mathcal{G} = \frac{1}{2B} e^{-(BA+\frac{A}{D+CA})} + \frac{e^{\frac{BD-1}{C}}}{2BC} \int_{E}^{\infty} e^{-\frac{s}{C}} \frac{s}{\sqrt{s^2+4BD}} ds. \tag{32}$$

The finite integral may be expressed as an infinite integral with the aid of the Meijer-G function [28], where the Meijer-G function is defined in [29] (9.301). Furthermore, $\frac{1}{\sqrt{s^2+4BD}}$ may also be expressed using the Meijer-G function [30](07.19.26.0002.01). Then we arrive at

$$\begin{aligned}\mathcal{G} =& \frac{1}{2B} e^{-(BA+\frac{A}{D+CA})} + \frac{e^{\frac{BD-1}{C}}}{4\Gamma(\frac{1}{2}) B^{\frac{3}{2}} C D^{\frac{1}{2}}} \\ &\times \int_{0}^{\infty} s e^{-\frac{s}{C}} G_{1,1}^{0,1}\left[\frac{s^2}{E^2} \middle| \begin{matrix} 1 \\ 0 \end{matrix} \right] G_{1,1}^{1,1}\left[\frac{s^2}{4BD} \middle| \begin{matrix} \frac{1}{2} \\ 0 \end{matrix} \right] ds. \end{aligned} \tag{33}$$

The product of two Meijer-G functions may be expressed as a single Meijer-G function associated with two variables [31, 32]. Using [33] Eq. (2.1), the final closed-form result is obtained as

$$\begin{aligned}\mathcal{G} =& \frac{1}{2B} e^{-(BA+\frac{A}{D+CA})} + \frac{C e^{\frac{BD-1}{C}}}{2\pi B^{\frac{3}{2}} D^{\frac{1}{2}}} \\ &\times S\left[\begin{matrix} \begin{pmatrix} 2,0 \\ 0,0 \end{pmatrix} \\ \begin{pmatrix} 0,1 \\ 1,1 \end{pmatrix} \\ \begin{pmatrix} 1,1 \\ 1,1 \end{pmatrix} \end{matrix} \middle| \begin{matrix} (1,\frac{3}{2}) \\ - \\ 1 \\ 0 \\ \frac{1}{2} \\ 0 \end{matrix} \middle| \begin{matrix} \\ \frac{(2C)^2}{E^2} \\ \\ \frac{(2C)^2}{(4BD)} \\ \\ \end{matrix} \right]. \end{aligned} \tag{34}$$

The corresponding MATHEMATICA code may be found in [32]. However, there are some bugs in this code. The correct code may be download from [34]. [4]

[4]In the code, 'Past', 'Qast', 'Qbst' and 'Mst' should contain both 'u' and 'v' and 'Ms[s]Mt[t]' is missing in the integral.

$$\mathcal{F} = T_{i,i+1} = \int_{\gamma_{SR}^{out2}}^{\infty} e^{-\gamma} \left(1 - e^{-\frac{1}{\frac{\bar{\gamma}_{SR}^{rec}}{\gamma} - \frac{\bar{\gamma}_{SR}^{rec}}{\gamma_{SR}^{out2}} + \frac{\bar{\gamma}_{RD}^{rec}}{-\ln\left(1 - \frac{T_{i,i}}{1-e^{-\gamma_{SR}^{out2}}}\right)}}} \right) d\gamma. \tag{35}$$

Finally, let $A = \gamma_{SR}^{out2}$, $B = 1$, $C = -\frac{\bar{\gamma}_{SR}^{rec}}{\gamma_{SR}^{out2}} + \frac{\bar{\gamma}_{RD}^{rec}}{-\ln\left(1 - \frac{T_{i,i}}{1-e^{-\gamma_{SR}^{out2}}}\right)}$ and $D = \bar{\gamma}_{SR}^{rec}$. Then the closed-form expression of $\mathcal{F}$ may be readily obtained.

2) $\mathcal{F}$ is a monotonically decreasing function of γ_{SR}^{out2}: Given the closed-form expression of (35), let us now prove that $\mathcal{F}$ is a monotonically decreasing function. In (35), the only unknown is γ_{SR}^{out2}. If we differentiate $\mathcal{F}$ with respect to γ_{SR}^{out2}, we arrive at:

$$\frac{d\mathcal{F}}{d\gamma_{SR}^{out2}} = -e^{-\gamma} \frac{T_{i,i}}{1 - e^{-\gamma_{SR}^{out2}}} < 0, \tag{36}$$

which shows that $\mathcal{F}$ is a monotonically decreasing function. Based on this property, γ_{SR}^{out2} may be found by searching from γ_{SR}^{out1} to infinity and stopping the search when (14) is satisfied. Then γ_{RD}^{out1} and E_{ffe} can be readily found.

REFERENCES

[1] M. O. Hasna and M.-S. Alouini, "Harmonic mean and end-to-end performance of transmission systems with relays," *IEEE Transactions on Communications*, vol. 52, no. 1, pp. 130 – 135, Jan. 2004.

[2] A. Muller and H.-C. Yang, "Dual-hop adaptive packet transmission systems with regenerative relaying," *IEEE Transactions on Wireless Communications*, vol. 9, no. 1, pp. 234 –244, Jan. 2010.

[3] M. Neely and E. Modiano, "Capacity and delay tradeoffs for ad hoc mobile networks," *IEEE Transactions on Information Theory*, vol. 51, no. 6, pp. 1917–1937, June 2005.

[4] A. El Gamal, J. Mammen, B. Prabhakar, and D. Shah, "Optimal throughput-delay scaling in wireless networks - part i: the fluid model," *IEEE Transactions on Information Theory*, vol. 52, no. 6, pp. 2568–2592, June 2006.

[5] L.-L. Yang, C. Dong, and L. Hanzo, "Multihop diversity-a precious source of fading mitigation in multihop wireless networks," in *IEEE Global Telecommunications Conference (Globecom'11), Houston, TX, USA*, Dec. 2011, pp. 1–5.

[6] C. Dong, L.-L. Yang, and L. Hanzo, "Multihop diversity for fading mitigation in multihop wireless networks," in *IEEE Vehicular Technology Conference (VTC'11-Fall), San Francisco, CA, USA*, Sept. 2011, pp. 1–5.

[7] N. Zlatanov, R. Schober, and P. Popovski, "Throughput and diversity gain of buffer-aided relaying," in *2011 IEEE Global Telecommunications Conference (GLOBECOM 2011)*, Dec 2011, pp. 1–6.

[8] C. Dong, L.-L. Yang, and L. Hanzo. [Online]. Available: http://eprints.soton.ac.uk/348686/

[9] N. Zlatanov, R. Schober, and P. Popovski, "Buffer-aided relaying with adaptive link selection," *IEEE Journal on Selected Areas in Communications*, vol. 31, no. 8, pp. 1530–1542, August 2013.

[10] N. Zlatanov and R. Schober, "Buffer-aided relaying with adaptive link selection-fixed and mixed rate transmission," *IEEE Transactions on Information Theory*, vol. 59, no. 5, pp. 2816–2840, 2013.

[11] G. Chen, Z. Tian, Y. Gong, Z. Chen, and J. Chambers, "Max-ratio relay selection in secure buffer-aided cooperative wireless networks," *IEEE Transactions on Information Forensics and Security*, vol. 9, no. 4, pp. 719–729, April 2014.

[12] C. Dong, L.-L. Yang, and L. Hanzo, "Multi-hop diversity aided multi-hop communications: A cumulative distribution function aware approach," *IEEE Transactions on Communications*, vol. 61, no. 11, pp. 4486–4499, 2013.

[13] ——, "Performance analysis of multi-hop diversity aided multi-hop links," *IEEE Transactions on Vehicular Technology*, vol. 61, no. 6, pp. 2504 –2516, 2012.

[14] B. Xia, Y. Fan, J. S. Thompson, and H. V. Poor, "Buffering in a three-node relay network," *IEEE Transactions on Wireless Communications*, vol. 7, no. 11, pp. 4492 –4496, Nov. 2008.

[15] V. Jamali, N. Zlatanov, and R. Schober, "Adaptive mode selection for bidirectional relay networks – fixed rate transmission," in *IEEE International Conference on Communications (ICC'14), Syndey, Australia*, Jun. 2014, pp. 1–5. [Online]. Available: http://arxiv.org/abs/1401.3520

[16] P. Zhang, S. Chen, and L. Hanzo, "Embedded iterative semi-blind channel estimation for three-stage-concatenated mimo-aided qam turbo transceivers," *IEEE Transactions on Vehicular Technology*, vol. 63, no. 1, pp. 439–446, 2014.

[17] S. Ten Brink, "Convergence behavior of iteratively decoded parallel concatenated codes," *IEEE Transactions on Communications*, vol. 49, no. 10, pp. 1727–1737, Oct 2001.

[18] M. El-Hajjar and L. Hanzo, "Exit charts for system design and analysis," *IEEE Communications Surveys Tutorials*, vol. 16, no. 1, pp. 127–153, First 2014.

[19] N. C. Beaulieu and J. Hu, "A closed-form expression for the outage probability of decode-and-forward relaying in dissimilar Rayleigh fading channels," *IEEE Communications Letters*, vol. 10, no. 12, pp. 813 –815, Dec. 2006.

[20] L. Hanzo, O. Alamri, M. El-Hajjar, and N. Wu, *Near-Capacity Multi-Functional MIMO Systems: Sphere-Packing, Iterative Detection and Cooperation*. Wiley IEEE Press, May 2009.

[21] L. Cheng, B. Henty, D. Stancil, F. Bai, and P. Mudalige, "Mobile vehicle-to-vehicle narrow-band channel measurement and characterization of the 5.9 ghz dedicated short range communication (dsrc) frequency band," *IEEE Journal on Selected Areas in Communications*, vol. 25, no. 8, pp. 1501–1516, Oct 2007.

[22] C. Dong, L.-L. Yang, J. Zuo, S. X. Ng, and L. Hanzo, "Energy, delay and outage analysis of a buffer-aided three-node network relying on opportunistic routing," *Accepted by IEEE Transactions on Communications*, 2015. [Online]. Available: http://eprints.soton.ac.uk/350501/

[23] C. Dong, J. Zuo, L.-L. Yang, Y. Huo, S. Ng, and L. Hanzo, "Energy-efficient buffer-aided relaying relying on non-linear channel probability space division," in *IEEE Wireless Communications and Networking Conference (WCNC'14), Istanbul, Turkey*, Apr. 2014, pp. 1–5.

[24] C. Dong, J. Zuo, L.-L. Yang, Y. Huo, S. X. Ng, and L. Hanzo, "On buffer-assisted opportunistic routing relying on linear transmission activation probability space partitioning for relay-aided networks," in *IEEE Vehicular Technology Conference (VTC'14-Fall), Vancouver, Canada*, Sep. 2014, pp. 1–5. [Online]. Available: http://eprints.soton.ac.uk/364724/

[25] C. Dong, L.-L. Yang, J. Zuo, S. Ng, and L. Hanzo, "Maximum throughput adaptive rate transmission scheme for multihop diversity aided multihop links," in *IEEE International Conference on Communications (ICC'14), Syndey, Australia*, Jun. 2014, pp. 1–5. [Online]. Available: http://eprints.soton.ac.uk/362139/

[26] D. Bertsekas and R. G. Gallager, *Data Networks, 2nd ed.* Prentice-Hall, Apr. 1992.

[27] I. Krikidis, T. Charalambous, and J. Thompson, "Buffer-aided relay selection for cooperative diversity systems without delay constraints," *IEEE Transactions on Wireless Communications*, vol. 11, no. 5, pp. 1957–1967, May 2012.

[28] V. Adamchic and O. Marichev, "The algorithm for calculating integrals of hypergeometric type functions and its realization in REDUCE system," in *Proc. Int. Conf. on Symbolic and Algebraic Computation*, 1990, pp. 212 –224.

[29] I. Gradshteyn and I. Ryzhik, *Table of Integrals, Series, and Products, Seventh Edition*. Elsevier Pte Ltd., 2007.

[30] *http://functions.wolfram.com/*.

[31] B. L. Sharma and R. F. A. Abiodun, "Generating function for generalized function of two variables," *Proc. American Mathematical Society*, vol. 46, no. 1, pp. 69 –72, Oct. 1974.

[32] I. S. Ansari, S. Al-Ahmadi, F. Yilmaz, M.-S. Alouini, and H. Yanikomeroglu, "A new formula for the BER of binary modulations with dual-branch selection over generalized-K channels," *IEEE Transactions on Communications*, vol. 59, no. 10, pp. 2654–2658, 2011.

[33] M. Shah, "On generalization of some results and their applications," *Collectanea Mathematica*, vol. 24, no. 3, pp. 249 –266, 1973.

[34] C. Dong, L. Li, B. Zhang, L.-L. Yang, and L. Hanzo, "Energy dissipation and delay tradeoffs in a buffer-aided two-hop link," *to be submitted*.